Parallel Low-Loss Measurement of Multiple Atomic Qubits

Minho Kwon,* Matthew F. Ebert, Thad G. Walker, and M. Saffman
Department of Physics, University of Wisconsin-Madison, 1150 University Avenue, Madison, Wisconsin 53706, USA
(Received 27 June 2017; published 30 October 2017)

We demonstrate low-loss measurement of the hyperfine ground state of rubidium atoms by state dependent fluorescence detection in a dipole trap array of five sites. The presence of atoms and their internal states are minimally altered by utilizing circularly polarized probe light and a strictly controlled quantization axis. We achieve mean state detection fidelity of 97% without correcting for imperfect state preparation or background losses, and 98.7% when corrected. After state detection and correction for background losses, the probability of atom loss due to the state measurement is $< 2\%$ and the initial hyperfine state is preserved with $> 98\%$ probability.

DOI: 10.1103/PhysRevLett.119.180504

Experiments with qubits encoded in hyperfine states of neutral atoms are being actively developed as a route towards scalable quantum information processing [1]. Several research groups have demonstrated preparation and control of order 50 qubits in 1D [2], 2D [3,4], and 3D [5] optical lattices. Quantum computation requires qubit state measurements to determine the result of a computation, and for measurement based quantum error correction [6]. Measurement of the quantum state of an atomic hyperfine qubit is most often performed by using a cycling, or near cycling, transition which repetitively transfers the qubit between a bright state $|B\rangle$ and an excited state $|e_B\rangle$. Detection of scattered photons due to illumination with light that is near resonant with the cycling transition projects the qubit into state $|B\rangle$. Conversely, if no photons are detected, the qubit is projected into the dark state $|D\rangle$. This idealized picture breaks down if the cycling transition is not perfectly closed, in which case an atom in state $|B\rangle$ may suffer a Raman transition to $|D\rangle$, thereby giving a measurement error.

Measurements that use a cycling transition rely on the availability of a metastable qubit dark state $|D\rangle$, or on shelving one of the qubit levels into a metastable dark state, as is done in trapped ion experiments [7]. In alkali atom experiments with qubits encoded in ground hyperfine levels the availability of a cycling transition generally relies on an angular momentum selection rule that is enforced by using probe light with a well-defined polarization. This implies that the probe light propagates along a single axis in space, which results in atomic heating due to the random direction of scattered photons. For a lossless measurement either the potential confining the atom should be sufficiently deep for the heating to be tolerable, as in experiments with ions [8], or the detection system should allow for a state measurement after scattering only a small number of photons to minimize heating. This latter approach was demonstrated with optically trapped atomic qubits [9–11] using single photon detectors.

There are several possible alternative measurement approaches including coupling of an atom to a high finesse cavity which enables state detection with minimal heating and without loss of atoms [12–14]. Superlattices with spin dependent potentials have been used for parallel measurement of atomic spin states [15]. It has been proposed to perform fast state measurements by coupling a single atom to a many atom ensemble, as a means of increasing the effective photon scattering rate [16]. It is also possible to enforce a dark state condition with three-dimensional probing light that cools the atoms, but this requires an inconvenient sequence of shelving steps [17].

In order to take full advantage of the large number of qubits available in neutral atom experiments, it is desirable to be able to losslessly measure multiple qubits in parallel. This can be done by imaging scattered light from an array of qubits onto a sensitive imaging detector such as an electron multiplying charge coupled device (EMCCD) camera. Although EMCCD cameras have high quantum efficiency, they suffer from excess readout noise which has hitherto rendered parallel lossless state detection infeasible. To circumvent this limitation previous array experiments used a "blow away" technique where atoms in $|B\rangle$ are ejected from the array using a single unbalanced beam, followed by detection of the presence or absence of an atom. Atom detection is performed using a 3D light field that cools the atoms, but does not prevent state changing Raman transitions during the measurement. This approach provides state measurements, but requires that a new atom has to be reloaded, half the time on average, which severely impacts the experimental data rate.

In this Letter we show that low-loss state detection of multiple atomic qubits is possible in parallel using an EMCCD camera. This requires a careful choice of parameters to minimize both the motional heating rate (which is lower at large detuning) and the Raman depumping rate (which is lower at small detuning). The enabling advances include use of a moderately high numerical aperture (NA = 0.4) collection lens, deep optical traps, and careful preparation of the polarization state of the probe light to minimize Raman transitions from $|B\rangle \rightarrow |D\rangle$.

The detection method is compatible with an ideal, projective measurement of the quantum state that leaves the atom in an eigenstate of $\hat{\sigma}_z$ (for neutral atom qubits a state of definite $|F, M_F\rangle$). Observation of the dark state $|D\rangle$ leaves the atomic state unchanged. If the bright state is encoded in $|F_+, M_F\rangle$, with F_+ the upper hyperfine state, observation of the bright state $|B\rangle$ leaves the atom in $|F_+, F_+\rangle$ for any initial M_F. The qubit can then be restored to $|F_+, M_F\rangle$ by following the detection of $|B\rangle$ with a sequence of rotations using stimulated Raman transitions or microwave pulses. The measurement can also be made cross talk free, a requirement for quantum error correction [18]. We emphasize that the experimental approach is compatible with quantum gate experiments in qubit registers [1], with no changes to the experimental apparatus. Since EMCCD cameras are available with up to 10^6 pixels the method demonstrated here has the potential for scaling to large arrays with thousands of atomic qubits. Similar results to ours have been independently reported in Ref. [22].

The experimental geometry and measurement sequence are shown in Fig. 1. Atoms are prepared in the $|F = 1\rangle$ or $|F = 2\rangle$ hyperfine levels of the ^{87}Rb $5s_{1/2}$ electronic ground state, corresponding to $|D\rangle$ and $|B\rangle$, respectively. Although qubits are defined in terms of specific hyperfine-Zeeman states $|1\rangle = |F_1, M_{F1}\rangle$ and $|0\rangle = |F_0, M_{F0}\rangle$ we use $|B\rangle$ and $|D\rangle$ here to represent random mixtures of the M_F states of the $F = 2$ and $F = 1$ hyperfine levels, respectively. The demonstration of measurement of states $|B\rangle$ and $|D\rangle$ also applies, without modification, to any pair of hyperfine-Zeeman states as long as they are attached to different hyperfine levels.

To prepare states of single atoms we start with a standard magneto-optical trap (MOT) that is then overlapped with a 1D array of five optical dipole traps (ODTs) formed by focusing 1040 nm light to a waist of w $\simeq 2.5$ μm. The traps are (2.8, 4.4, 5.6, 3.9, 3.4) mK deep and are spaced by $\sim$9 μm. The traps are pencil shaped with atomic density distributions of size (standard deviations) $\Delta_z, \Delta_r \sim 7.0, 0.7$ μm, with the long axis along the optical axis of the collection optics. Single atoms are loaded with probability 20%–30% at a temperature of $\sim$100 μK.

In order to measure the initial trap populations, the atoms are probed using 6 MOT beams with components near-resonant with $|B\rangle \leftrightarrow |e_B\rangle$ and $|D\rangle \leftrightarrow |e_D\rangle$ simultaneously, where $|e_B\rangle$ is the $F' = 3$ level and $|e_D\rangle$ is the $F' = 2$ level of the $5p_{3/2}$ excited state. Atom fluorescence is collected by a NA $= 0.4$ lens, and imaged onto an EMCCD camera (Andor iXon EM + DU-860). The magnification was chosen such that the site separation is 2 pixels, and the signal from each ODT is integrated over a region of interest (ROI) defined by 5 camera pixels, as shown in Fig. 2(a). We image each atom onto only a few pixels to minimize the electronic background noise incurred during camera readout. The excited states, $|e_B\rangle, |e_D\rangle$, are antitrapped in the ODT, so to avoid heating the atom we toggle the ODT and

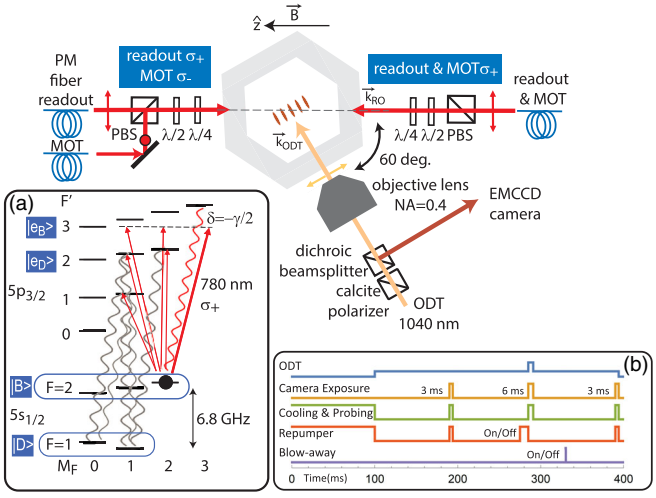

FIG. 1. Experimental setup around the hexagonal vacuum cell. For state readout σ_+ polarized light propagates along $\pm\vec{k}_{\mathrm{RO}}$, which is parallel to the quantization axis defined by the bias magnetic field $\vec{B}$. The trap light propagates along $\vec{k}_{\mathrm{ODT}}$ and a dichroic beam splitter separates the trap light and fluorescence light which is imaged onto the camera. Inset (a) shows the levels used for readout including the bright $|B\rangle$ and dark $|D\rangle$ hyperfine levels, and the corresponding excited state levels $|e_B\rangle$, $|e_D\rangle$. Inset (b) shows the experimental timing diagram.

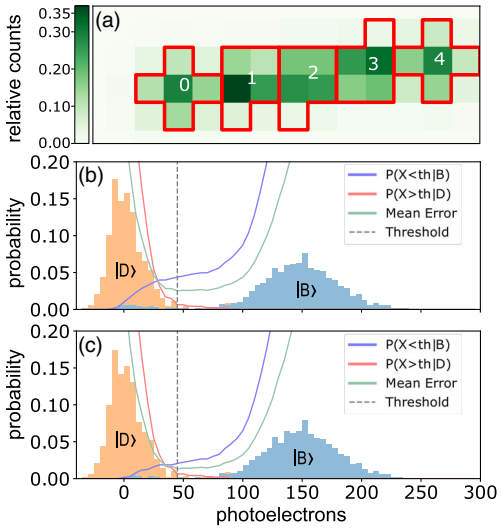

FIG. 2. (a) Regions of interest are five pixels enclosed by red borders with the relative photon counts on each pixel shown by the green shading. Each 5 pixel ROI receives (76,88,89,92,76)% of the light from the corresponding trapped atom. Neighboring site fluorescence cross talk is $\sim$2%. Each pixel represents a 4 μm $\times$ 4 μm area and the site-to-site separation is $\sim$9 μm. (b) Histograms of nondestructive readout in the central region (#2) for initial states $|B\rangle$ and $|D\rangle$. (c) The same data set postselected on the presence of an atom in the ROI in the third measurement, leaving only Raman depumping and state preparation as sources of error. Signals in histograms are background subtracted.

the probe beams out of phase with a 50% duty cycle at 1.25 MHz. The photon detection efficiency is estimated to be (1.6%–2.0%), accounting for the lens solid angle and dipole emission pattern (3.9%), transmission through optics (74%), EMCCD quantum efficiency ($\eta = 75\%$), and fluorescence lying outside of the camera pixels used to define regions of interest (76%–92%).

Upon completion of the population measurement, there is a 100 ms delay for image transfer to the computer, after which the atoms are initialized in a random superposition of the Zeeman substates of one of the hyperfine levels, chosen by leaving either $|D\rangle \leftrightarrow |e_D\rangle$ or $|B\rangle \leftrightarrow |e_B\rangle$ on to depopulate the coupled state. To prevent leakage light from disrupting the initialized states mechanical shutters block unwanted light after initialization is completed. We estimate the state preparation fidelity for both states to be $> 99.5\%$, limited by the fidelity of blow away measurements that are performed at reduced ODT depth.

After state initialization, a bias magnetic field $B_z \sim 20$ G making an angle of 60° from $\vec{k}_{\mathrm{ODT}}$, the long axis of the ODTs, is switched on. The probe beams propagate along and counter to $\vec{k}_{\mathrm{RO}}$, which is set to be parallel to $\hat{z}$ with a possible small alignment error θ. We use counterpropagating probe beams to mitigate the effect of heating due to near-resonant radiation pressure. In order to suppress Raman transitions both readout beams are σ_+ polarized which optically pumps the atoms into the lower state of the $|2,2\rangle \leftrightarrow |3',3'\rangle$ cycling transition. The counterpropagating probe beams are generated from separate lasers with a relative frequency offset of 500 kHz. This technique avoids standing wave patterns, which can cause a time dependent drift in the single atom scattering rate thereby broadening the camera signal distribution. During the state measurement sequence the trap depths are temporarily doubled to enhance retention of the atoms. The probe beams are set to saturation parameter $s_0 = 1$ (summed over both beams) and detuning $\delta = -(\gamma/2)$ red of the Zeeman shifted $|2,2\rangle \leftrightarrow |3',3'\rangle$ transition to provide maximal motional damping [23] with γ the excited state linewidth. The atoms are illuminated for 6 ms with the same 50% duty cycle as is used for the population measurement and fluorescence light is collected by the EMCCD for analysis. The resulting data are shown in Fig. 2. The hyperfine state is determined on the basis of a simple threshold condition relative to the vertical dashed lines in Figs. 2(b),2(c). Although more extensive analysis that utilizes information gained from the temporal or spatial distribution of light in each ROI can further reduce uncertainties [7,22], our results show that the threshold condition alone is adequate for high fidelity measurements.

After an additional 100 ms delay for image transfer, a third readout sequence probes the atoms again. Depending on the experiment, the third readout is either a second population measurement for probing atom loss or a destructive state selective measurement using a blow away beam for measuring the number of atoms depumped from $|B\rangle$ to $|D\rangle$. Full characterization of the nondestructive measurement requires 4 experiments: 2 (state preparation $|B\rangle$ or $|D\rangle$) ×2 (blow away on or off). The results of the 4 experiments are summarized in Table I for the center site and Table II for the other sites. We note that the results marked with (a) include 2% atom loss between each camera readout due to the finite trap lifetime $\tau \sim 5$ s and the 100 ms gap between each measurement. The background collision loss is not a fundamental limitation, and could be reduced by decreasing the chamber pressure or by shortening the image transfer time.

TABLE I. Results in the central site (#2) averaged over 2000 measurements. Data marked (a) are without correction, and data marked (b) are postselected on the presence of an atom in the ROI in the third measurement, leaving only Raman depumping and state preparation as sources of error. The final state results are found from a third, state-selective measurement using a blow away beam.

	Detected state (%)		Final state (%)		
Initial state	$\|B\rangle$	$\|D\rangle$	$\|B\rangle$	$\|D\rangle$	Lost
$\|B\rangle$	(a) 95.6(6)	(a) 4.4(6)	98.6(1.9)	0.6 (1.6)	0.8(1.3)
	(b) 98.0(4)	(b) 2.0(4)			
$\|D\rangle$	0.6(4)	99.4(4)	N/A	99.6(1.6)	0.4 (1.6)

The primary limitation to the nondestructive measurement is the mean number of photons N_γ that can be scattered before the atom is depumped from $|B\rangle$ to $|D\rangle$. When using random polarization $N_\gamma = 38\,340/(1 + 4\delta^2/\gamma^2 + s_0)$, where $s_0 = I/I_{\mathrm{s,eff}}$ and $I_{\mathrm{s,eff}} = 3.6$ mW/cm^2 is the saturation parameter for randomly polarized light; see Ref. [18] for a derivation. With typical experimental parameters 10^4 photons could be scattered, which would lead to approximately 100 photoelectrons, which is technically enough to clearly resolve the $|B\rangle$ and $|D\rangle$ photon histograms. However, the $|B\rangle$ state histogram would leave a long tail from depumping events during the exposure that would overlap with the $|D\rangle$ state distribution. Therefore, in order to obtain clearly distinguishable photoelectron statistics we need the additional constraint that atoms scatter $\sim 10^4$ photons with minimal depumping, a condition that isotropic polarization does not satisfy.

TABLE II. Loss-corrected detection fidelities for the outer four traps. $|\psi\rangle_i$ is the prepared state.

	Detection fidelity (%)			
ROI	No. 0		No. 1	
$\|\psi\rangle_i$	$\|B\rangle$	$\|D\rangle$	$\|B\rangle$	$\|D\rangle$
$\|B\rangle$	97.1(5)	2.9(5)	98.3(3)	1.7(3)
$\|D\rangle$	0(0)	100(0)	1.0(5)	99.0(5)
	No. 3		No. 4	
$\|\psi\rangle_i$	$\|B\rangle$	$\|D\rangle$	$\|B\rangle$	$\|D\rangle$
$\|B\rangle$	97.7(6)	2.3(6)	98.2(1.2)	1.8(1.2)
$\|D\rangle$	0.5(4)	99.5(4)	0	100(0)

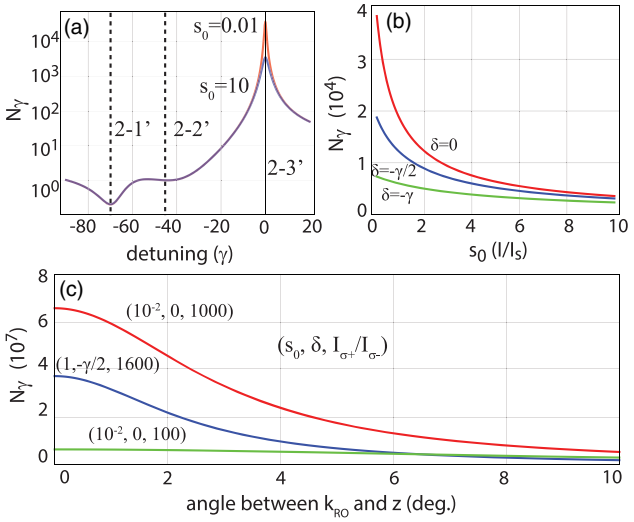

FIG. 3. Dependence of the mean number of resonant photons per Raman photon on probe light parameters. (a) Detuning dependence spanning neighboring levels. (b) Intensity dependence at three different detunings. (c) Enhancement with σ polarized light for given saturation, detuning, and intensity contrast $I_{\sigma_+}/I_{\sigma_-}$ between σ_+ and σ_-.

To suppress the depumping we have used σ_+-polarized light along the quantization axis to pump the atoms into $|2,2\rangle$, the lower level of the cycling transition as described above. In an actual experiment there is still a finite depumping rate due to polarization impurity or a small angular mismatch θ between $\hat{z}$, the direction of the magnetic field, and $\vec{k}_{\mathrm{RO}}$, the axis of the readout beams. The figure of merit is the number of photons that the bright state can scatter before it falls into the dark state, as shown in Fig. 3. We can quantify the probability of depumping by summing the rates over Raman depumping channels and comparing to the scattering rate on the cycling transition [18]. We estimate that we are able to scatter $N_{\gamma,\sigma} = 3.7 \times 10^5$ photons corresponding to an enhancement factor of $\sim$20 over the unpolarized case with parameters $s_0 = 1$, $\delta = -\gamma/2$ and measured polarization purity $I_{\sigma_+}/I_{\sigma_-} = 1600$ [18]. There is also a small transient contribution to the depumping probability as the atoms are pumped from the initial state towards $|2,2\rangle$, which is estimated in Ref. [18].

It is also necessary to account for depumping due to the vector and tensor light shifts imposed by the ODT. Circular polarization of the ODT light results in a vector shift on the atoms which adds a fictitious magnetic field, $\vec{B}_{\mathrm{fict}}$, along $\vec{k}_{\mathrm{ODT}}$. The 60° angle between $\vec{k}_{\mathrm{ODT}}$ and $\vec{k}_{\mathrm{RO}}$ drives Larmor precession, which reopens the depumping channels. In terms of the trap depth U_0 the fictitious field is $\vec{B}_{\mathrm{fict}}/U_0 = 29.77\mathcal{A}\alpha^{(1)}_{|B\rangle}\hat{k}_{\mathrm{ODT}}/\alpha^{(0)}_{|B\rangle}$ (G/mK) [18], with $\alpha^{(0)}_{|B\rangle}$, $\alpha^{(1)}_{|B\rangle}$ the scalar and vector polarizabilities, and $-1 \le \mathcal{A} \le 1$ the degree of circular polarization. For our experimental parameters, $\mathcal{A} \sim 2 \times 10^{-4}$, $\lambda_{\mathrm{ODT}} = 1040$ nm, $\vec{B}_{\mathrm{fict}}/U_0 = 0.3$ mG/mK. To mitigate depumping from $\vec{B}_{\mathrm{fict}}$ we used a bias field of $B_z \sim 20$ G, such that the depumping rate was independent of ODT power [18], which shows that the vector light shift did not cause additional depumping for our parameters.

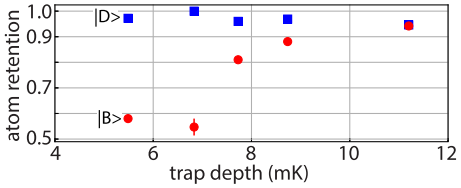

FIG. 4. Probability of atom retention after nondestructive readout as a function of trap depth during the readout phase. Background gas collisions cause $\sim$4% atom loss between the first and third measurements.

In addition, excited state tensor light shifts couple M'_F states, creating a new set of energy eigenstates that are superpositions of $|F', M'_F\rangle$ states, which breaks the cycling character of the $|2,2\rangle \leftrightarrow |3',3'\rangle$ transition. To avoid tensor shifts during readout the probe and ODT lights are chopped out of phase so that the excited state is never populated when the ODT is on.

Despite the use of counterpropagating σ_+ beams, heating was still noticeable, limiting atom retention after the measurement, as is shown in Fig. 4, and forcing us to use traps that are $\sim$10 mK deep. This limited performance may be attributed to laser intensity noise, lack of sub-Doppler cooling mechanisms, and 1D cooling. Future improvements including working with a higher NA lens to improve photon collection efficiency, and cooling the atoms into the Lamb-Dicke regime to suppress recoil heating will further reduce atom loss. Using blue detuned traps with intensity minima at the location of the atoms, as in Refs. [5,24], would reduce the excited state tensor mixings, and obviate the need to turn the ODT on and off, thereby reducing any heating due to trap switching.

In conclusion, we have demonstrated nondestructive parallel readout of an array of five Rb atoms. Increasing the collection efficiency of the imaging optics, combined with colder atoms, and possibly more refined analysis of the spatial information provided by the camera, we anticipate that loss of atoms due to heating can be reduced to a level compatible with implementation of repetitive error correction for quantum computation.

This work was supported by NSF Grant No. 1521374, the AFOSR Quantum memories MURI, and the ARL-CDQI through cooperative agreement W911NF-15-2-0061. M. S. thanks Dieter Meschede for sharing their results prior to publication.

*mkwon22@wisc.edu

[1] M. Saffman, Quantum computing with atomic qubits and Rydberg interactions: Progress and challenges, J. Phys. B **49**, 202001 (2016).

[2] M. Endres, H. Bernien, A. Keesling, H. Levine, E. R. Anschuetz, A. Krajenbrink, C. Senko, V. Vuletic, M. Greiner, and M. D. Lukin, Atom-by-atom assembly of defect-free one-dimensional cold atom arrays, Science **354**, 1024 (2016).

[3] T. Xia, M. Lichtman, K. Maller, A. W. Carr, M. J. Piotrowicz, L. Isenhower, and M. Saffman, Randomized Benchmarking of Single-Qubit Gates in a 2D Array of Neutral-Atom Qubits, Phys. Rev. Lett. **114**, 100503 (2015).

[4] D. Barredo, S. de Leséléuc, V. Lienhard, T. Lahaye, and A. Browaeys, An atom-by-atom assembler of defect-free arbitrary two-dimensional atomic arrays, Science **354**, 1021 (2016).

[5] Y. Wang, A. Kumar, T.-Y. Wu, and D. S. Weiss, Single-qubit gates based on targeted phase shifts in a 3D neutral atom array, Science **352**, 1562 (2016).

[6] S. J. Devitt, W. J. Munro, and K. Nemoto, Quantum error correction for beginners, Rep. Prog. Phys. **76**, 076001 (2013).

[7] A. H. Myerson, D. J. Szwer, S. C. Webster, D. T. C. Allcock, M. J. Curtis, G. Imreh, J. A. Sherman, D. N. Stacey, A. M. Steane, and D. M. Lucas, High-Fidelity Readout of Trapped-Ion Qubits, Phys. Rev. Lett. **100**, 200502 (2008).

[8] H. Häffner, C. F. Roos, and R. Blatt, Quantum computing with trapped ions, Phys. Rep. **469**, 155 (2008).

[9] M. J. Gibbons, C. D. Hamley, C.-Y. Shih, and M. S. Chapman, Nondestructive Fluorescent State Detection of Single Neutral Atom Qubits, Phys. Rev. Lett. **106**, 133002 (2011).

[10] A. Fuhrmanek, R. Bourgain, Y. R. P. Sortais, and A. Browaeys, Free-Space Lossless State Detection of a Single Trapped Atom, Phys. Rev. Lett. **106**, 133003 (2011).

[11] Y.-Y. Jau, A. M. Hankin, T. Keating, I. H. Deutsch, and G. W. Biedermann, Entangling atomic spins with a Rydberg-dressed spin-flip blockade, Nat. Phys. **12**, 71 (2016).

[12] J. Bochmann, M. Mücke, C. Guhl, S. Ritter, G. Rempe, and D. L. Moehring, Lossless State Detection of Single Neutral Atoms, Phys. Rev. Lett. **104**, 203601 (2010).

[13] J. Volz, R. Gehr, G. Dubois, J. Estève, and J. Reichel, Measurement of the internal state of a single atom without energy exchange, Nature (London) **475**, 210 (2011).

[14] H. Zhang, R. McConnell, S. Ćuk Q. Lin, M. H. Schleier-Smith, I. D. Leroux, and V. Vuletić, Collective State Measurement of Mesoscopic Ensembles with Single-Atom Resolution, Phys. Rev. Lett. **109**, 133603 (2012).

[15] M. Boll, T. A. Hilker, G. Salomon, A. Omran, J. Nespolo, L. Pollet, I. Bloch, and C. Gross, Spin- and density-resolved microscopy of antiferromagnetic correlations in Fermi-Hubbard chains, Science **353**, 1257 (2016).

[16] M. Saffman and T. G. Walker, Entangling single- and N-atom qubits for fast quantum state detection and transmission, Phys. Rev. A **72**, 042302 (2005).

[17] I. I. Beterov and M. Saffman, Rydberg blockade, Förster resonances, and quantum state measurements with different atomic species, Phys. Rev. A **92**, 042710 (2015).

[18] See Supplemental Material at http://link.aps.org/supplemental/10.1103/PhysRevLett.119.180504 for analysis of qubit shelving, photoelectron statistics, camera noise, and atomic state dynamics with dependencies on experimental parameters. The Supplemental Material includes Refs. [3,17,19–21].

[19] M. Hirsch, R. J. Wareham, M. L. Martin-Fernandez, M. P. Hobson, and D. J. Rolfe, A stochastic model for electron multiplication charge-coupled devices—from theory to practice, PLoS One **8**, 1 (2013).

[20] A. Hyvärinen and E. Oja, Independent component analysis: algorithms and applications, Neural Netw. **13**, 411 (2000).

[21] M. Martínez-Dorantes, Ph.D. thesis, Rheinischen Friedrich-Wilhelms-Universität Bonn, 2016.

[22] M. Martinez-Dorantes, W.Alt, J. Gallego, S. Ghosh, L. Ratschbacher, Y. Völzke, and D. Meschede, Nondestructive Parallel Readout of Neutral Atom Registers in Optical Potentials, proceeding Letter, Phys. Rev. Lett. **119**, 180503 (2017).

[23] D. J. Wineland and W. M. Itano, Laser cooling of atoms, Phys. Rev. A **20**, 1521 (1979).

[24] M. J. Piotrowicz, M. Lichtman, K. Maller, G. Li, S. Zhang, L. Isenhower, and M. Saffman, Two-dimensional lattice of blue-detuned atom traps using a projected Gaussian beam array, Phys. Rev. A **88**, 013420 (2013).